netic ordering near 14°K. The entropy associated with our observed peak in C_p at 13.3°K is strikingly close to the value $\frac{1}{2}R\ln 2$, which is difficult to dismiss as purely coincidental. Between 2.5 and 10°K $C_M \sim T^4$ is fairly well obeyed. It is suggested that the rhombohedral lattice of samarium is the key to the problem and that the lattice specific heat of this metal cannot very well be approximated by C_L(La). The sharp peak at 9.6°K is probably due to traces of some impurity which undergoes a magnetic transition at that temperature.

Most of the observations in this work can be correlated with results from other properties of the metals, such as magnetic susceptibility and electrical resistivity. In comparison with previous specific-heat measurements covering the range from 3–25°K, the present work gives more accurate results, owing to improved techniques and higher-purity specimens.

ACKNOWLEDGMENTS

We wish to express our thanks to D. W. Osborne, H. E. Flotow, and F. Schreiner for lending us a germanium resistance thermometer for calibration purposes. The help of Zenon Sungaila in preparing the cryostat for these experiments is gratefully acknowledged. L. J. S. wishes to thank Finland's Federation of University Women for a research grant.

PHYSICAL REVIEW VOLUME 158, NUMBER 3 15 JUNE 1967

Kinetics of Oxide Film Growth on Metal Crystals: Electron Tunneling and Ionic Diffusion

A. T. Fromhold, Jr., and Earl L. Cook*
Department of Physics, Auburn University, Auburn, Alabama
(Received 28 December 1966)

Numerical computations have been made for the growth rate of oxide and other dielectric contact films for the case of ion transport by diffusion and electron transport by tunneling. In the early phase of growth, electronic equilibrium prevails and the oxide growth rate can be limited by the diffusion of ions aided by a relatively large negative electrical contact potential V_M between metal and adsorbed oxygen. In the later phase of growth, ionic equilibrium prevails and the rate can be limited by the tunneling of electrons through the oxide aided by a positive electrical ionic diffusion potential V_D. The growth law in the early phase is of the Mott-Cabrera form, while in the later phase it is very nearly direct-logarithmic. The rather sharp transition between the two growth laws occurs at film thicknesses of the order of 20 to 30 Å, and is accompanied by a change in sign of the electrical potential across the oxide. The oxide growth rate in the early stages depends primarily on the value of the Mott potential V_M (defined as the difference in metal Fermi level and the O^- level in adsorbed oxygen) and the parameters associated with ionic diffusion. For the later stages of growth, the metal-oxide electronic work function χ_0 is the most important parameter, with the ratio of ionic boundary concentrations playing a lesser role through V_D. An increase in temperature increases the growth rate exponentially in the early growth stages, but increases the rate only moderately through V_D in the later stages.

I. INTRODUCTION

In 1939 Mott proposed a model[1,2] to explain the limiting-thickness behavior of the growth kinetics of thin oxide films on metals. The model was for low-temperature oxidation; the thermal excitation of electrons from the metal into the conduction band of the oxide was thus considered to be unimportant, so that electrons could penetrate the film only by the quantum-mechanical tunnel effect.[3,4] The electron current J_e could thus be large only for oxide films less than a few tens of angstroms in thickness. The metal ions were considered to diffuse[5] through the oxide film, however, so that the temperature had to be high enough to allow some thermal motion of the ions. Therefore, the limits of applicability of this model are that the thermal energy kT must be sufficiently low relative to the metal-oxide work function to eliminate thermionic emission but large enough relative to the activation energy for ionic diffusion to allow thermal motion of ions. This requires in general that the electron metal-oxide work function χ_0 for the system be larger than the activation energy W for ionic motion, assuming no drastic differences in the pre-exponential factors.

Neglecting the effect of electric fields, the ionic current for this model according to Mott is given by

$$J_i = -D_i dC_i/dx, \tag{1.1}$$

* National Aeronautics and Space Administration Predoctoral Fellow.

[1] N. F. Mott, Trans. Faraday Soc. **35**, 1175 (1939).
[2] N. F. Mott, Trans. Faraday Soc. **36**, 472 (1940).
[3] J. Frenkel, Phys. Rev. **36**, 1604 (1930).
[4] A. Sommerfeld and H. Bethe, *Handbuch der Physik*, edited by H. Geiger and K. Scheel (Springer, Berlin, 1933), Vol. XXIV/2, p. 450.
[5] W. Jost, *Diffusion* (Academic Press Inc., New York, 1952).

which in the steady-state[6] decreases inversely with increasing film thickness $L(t)$. The parameter D_i is the diffusion coefficient,[5] C_i is the concentration of the diffusing ionic species (apart from the stoichiometric concentration), and x is the position normal to the metal-oxide interface, at which $x=0$. The corresponding electronic current according to Mott is given by

$$J_e=A' \exp\{-L(t)/L_c\}, \quad (1.2)$$

which decreases nearly exponentially with increasing $L(t)$. The parameter A' is a slowly varying function[7–9] of $L(t)$ which has a value of the order of 10^{26} particles/cm^2 sec, and L_c represents a critical thickness[2] (of the order of several angstroms) at which the film begins to attenuate the electron tunnel current markedly.

$$A'=\chi_0/4\pi^2\hbar L(t)^2, \quad (1.3)$$

$$L_c=\hbar(8m\chi_0)^{-1/2}. \quad (1.4)$$

The parameter χ_0 is the metal-oxide work function, m is the effective mass of the electron, and $\hbar$ is the ratio of Planck's constant h to 2π.

The growth rate $dL(t)/dt$ was considered by Mott to be given by R_cJ_c, where J_c is the smaller of the two currents. The parameter R_c is defined as the volume of oxide formed per particle of the rate-limiting species which reaches the oxide-oxygen ($x=L(t)$) interface. The picture of the growth kinetics which emerges from this model is quite simple: The thermal diffusion of ions limits the growth rate for films so thin that the electron tunnel current J_e is larger than the ionic diffusion current J_i, and this stage of growth is parabolic ($L(t)^2\propto t$). On the other hand, the electronic current J_e limits the growth rate in thicker films, for which J_e is smaller than J_i, and this stage of growth is nearly direct-logarithmic ($L(t)\propto \log t$).

Mott formulated a second model (published[10] in 1947) which was subsequently expanded and elaborated upon by Cabrera and Mott[11] in 1949. This second model, often referred to as the Mott-Cabrera theory, is somewhat less restrictive in range of temperature and film thickness since it is based on thermionic emission of electrons (or perhaps electron tunneling, according to Cabrera and Mott[11]) and ionic diffusion. The following two characteristics distinguish the second model from the first model:

(a) Electrons were considered to traverse the film, either by thermionic emission from the metal into the conduction levels of the oxide or by the tunnel effect, more rapidly than ions could diffuse through the film. An equilibrium electrical contact-potential V_M was considered to be established in this manner between the metal and oxygen adsorbed on the oxide.

(b) A large uniform electric field $E_0=-V_M/L(t)$ both in the oxide and at the metal-oxide interface due to the contact potential V_M could lower the energy barriers for the initiation of ionic motion in the forward direction by an amount sufficient to yield a large contribution to ionic diffusion, even if the temperature is so low that ordinary diffusion given by Eq. (1.1) is negligible.

The lowering of the energy barriers for ionic motion discussed by Mott[10] for large macroscopic electric fields in the oxide is herein termed "nonlinear diffusion," whereas ordinary diffusion[5] combined with the low-field limiting case of the mobility current linearly dependent on electric field is termed "linear diffusion." The equation of Mott,[10,11] based on the assumption that nonlinear diffusion under the aiding potential V_M is rate-limiting, is

$$J_i=2n_i\nu \exp(-W/kT)\sinh(-q_iaV_M/kTL), \quad (1.5)$$

where n_i is the number of ions per unit area which are in a position to jump the rate-limiting energy barrier W, ν is the ionic attempt frequency, $2a$ is the ionic jump distance, q_i is the charge per particle of the diffusing ionic species, k is the Boltzmann constant, and T is the absolute temperature. Equation (1.5) is equally valid whether the rate-limiting barrier W is at the metal-oxide interface or inside the oxide film. The quantity n_i is frequently expressed in terms of a bulk concentration C_i for the diffusing species, in which case $n_i=2aC_i$.

The electrical contact potential V_M, designated herein as the "Mott potential," is given by the initial difference in the metal Fermi level and the oxygen O^- level, being negative in sign whenever the O^- level lies below the Fermi level of the metal. Figure 1 represents an energy diagram for electrons in the metal-oxide-oxygen system. Note that the metal-vacuum work function is ϕ_0 (subscript designating $x=0$), and the metal-oxide work function (energy difference between the conduction band in the oxide and the Fermi level in the metal) is χ_0. The difference between the vacuum potential and the O^- level in the adsorbed oxygen is represented by ϕ_L [subscript designating $x=L(t)$]; the corresponding energy difference between the conduction band in the

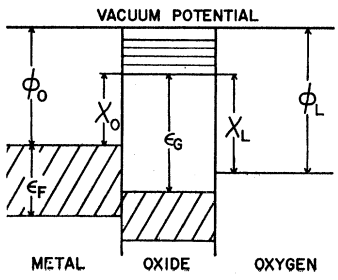

FIG. 1. Energy-level diagram for metal-oxide-oxygen system.

[6] A. T. Fromhold, Jr., J. Phys. Chem. Solids 24, 1081 (1963).
[7] J. G. Simmons, J. Appl. Phys. 34, 2583 (1963).
[8] R. Stratton, J. Phys. Chem. Solids 23, 1177 (1962).
[9] T. E. Hartman and J. S. Chivian, Phys. Rev. 134, A1094 (1964).
[10] N. F. Mott, Trans. Faraday Soc. 43, 431 (1947).
[11] N. Cabrera and N. F. Mott, Rept. Progr. Phys. 12, 163 (1949).

oxide and the O^- level in the adsorbed oxygen is represented by χ_L. The width of the filled portion of the conduction band in the metal is designated ϵ_F, and the band gap in the oxide is ϵ_G. The Mott potential V_M is herein defined as

$$V_M = e^{-1}(\chi_0 - \chi_L), \tag{1.6}$$

which from Fig. 1 can be seen to be equal to $e^{-1}(\phi_0 - \phi_L)$, where e is the *magnitude* of the electronic charge. For the potential energy diagram in Fig. 1, V_M is negative in sign. An equilibration of the metal Fermi level and the oxygen O^- level by electron transfer from metal to oxygen results in the establishment of an electrostatic potential V_M across the oxide film, so that a positive electric field E, equal to $E_0 = -V_M/L(t)$ in the absence of space charge, is created in the oxide. Figure 1 is an idealized representation of the energy, since image effects actually round the sharp discontinuities in potential at the interfaces.

Cabrera[12] has shown that electromagnetic radiation corresponding to energies as large as χ_0 and χ_L can shift the electron equilibrium so that an electrostatic potential somewhat greater in magnitude than V_M can thereby be established across the film. This is essentially due to the fact that the effective density of electronic states for photon excitation are different at the two interfaces. Cabrera[12] has also deduced that a flux of molecular oxygen from the gas phase sufficient to maintain V_M during oxidation requires oxygen pressures of the order of 10^{-4} Torr or larger. In addition, Grimley[13] has argued that equilibrium adsorption isotherms require that V_M should be temperature- and pressure-dependent, although these effects are predicted to be rather small at ordinary temperatures and oxygen pressures.

The present paper represents a synthesis of the two theories of Mott[1,2,10] (and the theory of Mott and Cabrera[11]) in the domain where electron transport occurs by tunneling.[14] All essential features are included; in addition, the following are incorporated into the model:

(a) The effect of the ionic concentration gradient on the nonlinear diffusion current.

(b) The effect of the ionic diffusion potential on the electron tunnel current.

(c) The capability of an electrical current equilibrium for either of the two charged species.

Numerical analysis of the model has been performed; the results which are presented here illustrate the predicted kinetics of growth and delineate the effects of the several parameters in low-temperature oxidation phenomena.

The technique used for obtaining the growth rate is that of coupled charge currents[6,15] first proposed by Wagner[16] and applied to the derivation of the parabolic growth law[15,16] for transport by electronic and ionic diffusion. In the present case, the surface-charge field is determined from the condition[15] of equal charge currents of the oppositely charged species and the growth rate $dL(t)/dt$ is then obtained by evaluating one of the currents as a function of film thickness.

Our results[17] show an early-stage Mott-Cabrera type law, corresponding to film growth which is rate-limited by ionic diffusion, and a later-stage direct-logarithmic law, corresponding to film growth which is rate-limited by electron-tunneling. These laws are the same ones obtained by Mott for the second and the first models, respectively; our rate constant for the direct-logarithmic law, however, is modified by the electric field in the film. In addition, our work represents a quantitative determination of the transition[18] between the limiting cases of a current equilibrium for one of the two species.

II. FORMULATION OF EQUATIONS

1. Ion (or Ion-Vacancy) Current

The ionic diffusion current J_i, in the absence of space-charge effects,[19,20] is given[21] in the steady-state approximation by

$$J_i = 4av \exp(-W/kT)\sinh(Z_i e E_0 a/kT) \times \{C_i(L) - C_i(0)\exp[Z_i e E_0 L(t)/kT]\}/ \{1-\exp[Z_i e E_0 L(t)/kT]\}. \tag{2.1}$$

The parameters $C_i(L)$ and $C_i(0)$ are the bulk-defect concentrations of the diffusing ionic species (interstitials or vacancies) at the oxide-oxygen ($x=L$) and at the metal-oxide ($x=0$) interfaces, respectively, while E_0 is the surface-charge field in the oxide. The parameter e is the magnitude of the electronic charge, and $Z_i e$ is the *effective charge* per particle of the ionic species undergoing transport through the lattice.[21] The Z_i includes sign of the charge, covalency, and internal electric-field effects, and thus $Z_i e$ differs in general from q_i, which is considered here to be the actual electric charge (includ-

[12] N. Cabrera, Phil. Mag. **40**, 175 (1949).

[13] T. B. Grimley, Disc. Faraday Soc. **28**, 223 (1959); T. B. Grimley and B. M. W. Trapnell, Proc. Roy. Soc. (London) **A234**, 405 (1956).

[14] The thermionic emission case is distinctly different; hence, it is not included in the present paper. A treatment of the electron rate-limited phase of the thermionic emission case has been presented: A. T. Fromhold, Jr., and Earl L. Cook, Phys. Rev. Letters **17**, 1212 (1966).

[15] A. T. Fromhold, Jr., J. Phys. Chem. Solids **24**, 1309 (1963); Bull. Am. Phys. Soc. **10**, 454 (1965); J. Chem. Phys. **41**, 509 (1964).

[16] C. Wagner, Z. Physik. Chem. **B21**, 25 (1933).

[17] Our results for the limiting case of a linear ionic diffusion current have been reported: A. T. Fromhold, Jr. and Earl L. Cook, Bull. Am. Phys. Soc. **11**, 195 (1966).

[18] A. T. Fromhold, Jr. and Earl L. Cook, J. Chem. Phys. **44**, 4564 (1966).

[19] A. T. Fromhold, Jr., J. Phys. Chem. Solids **25**, 1129 (1964).

[20] A. T. Fromhold, Jr., J. Chem. Phys. **40**, 3335 (1964).

[21] A. T. Fromhold, Jr. and Earl L. Cook, J. Appl. Phys. (to be published). This equation is based on a discrete picture of the lattice; it is somewhat similar to the integrated form of a continuum equation given by L. Young, *Anodic Oxide Films* (Academic Press Inc., New York, 1961), p. 16.

ing magnitude and sign) that is transported by one defect which diffuses from one interface of the oxide film to the opposite interface. The quantity Z_ie determines the force exerted on a diffusing defect by a given value of the macroscopic electric field and is the quantity which occurs in the Einstein relation, while q_i is a measure of the *actual* electric charge associated with the diffusing defect. Space-charge effects,[19,20] however, are neglected in the present treatment because of the thinness of the films involved in electron tunneling. This is a good approximation[19–21] for charged defect concentrations below $10^{17}/\text{cm}^3$ whenever the film thickness is less than 50 Å.

For cases in which a negative Mott potential V_M exists across the film, the sign of the field is positive. For the case of diffusing cation interstitials, $C_i(0)>C_i(L)$ and the sign of Z_i is also positive; the quantity $Z_ieE_0L(t)/kT$ is therefore a positive quantity much greater than unity for this case, since eV_M is generally expected to be of the order of an electron volt while kT is of the order of 0.03 eV. Equation (2.1) reduces very closely in this limit to the equation of Mott for nonlinear diffusion, Eq. (1.5), provided that Z_ie equals q_i and $2aC_i(0)$ is substituted for n_i. The additional approximation suggested by Mott[10,11] of replacing the hyperbolic sine function by $\pm\frac{1}{2}\exp|Z_ieE_0a/kT|$ will also be valid for Eq. (2.1) provided that E_0 is much greater in magnitude than $|kT/Z_iea|$. For a monovalent ion diffusing in an oxide with a lattice constant $2a$ of 5 Å, $|kT/Z_iea|$ is approximately 10^6 V/cm at 300°K.

Equation (2.1) is quite general, since it still provides a valid description of the current whenever the potential across the film is much less than V_M, and even when it has the opposite polarity from a negative V_M. This generality is necessary, since the growth rate can be either ion or electron rate limited, and in fact undergoes a transition between the two cases as the oxide film increases to a thickness which severely attenuates the electron tunnel current.

The ionic current J_i approaches zero as the built-in homogeneous field E_0 in Eq. (2.1) approaches $E_{\max}{}^{(i)}$,

$$E_{\max}{}^{(i)}=\{kT/Z_ieL(t)\}\ln\{C_i(L)/C_i(0)\}. \quad (2.2)$$

This is the largest field (in magnitude) which can be created by the diffusing ionic species; it corresponds to a current equilibrium of the ionic species. This means that at any point in the film the ionic current in one direction due to the concentration gradient is equal to the ionic current in the opposite direction due to the electric field created by the full ionic diffusion potential $V_D=-LE_{\max}{}^{(i)}$, with $E_{\max}{}^{(i)}$ given by Eq. (2.2). The quantity V_D is positive in sign, which corresponds to a negative field in the oxide. Although this diffusion potential is thermodynamically equivalent to an electrical potential insofar as both represent a capability to transport charged particles, the microscopic origins are different; an electric field exerts a direct force on each charged particle undergoing random thermal motion, while no such direct force acts on each particle in the case of a concentration gradient. In the present case the diffusion potential provides one source for the electric field E_0.

For values of E_0 much less in magnitude than $|kT/Z_iea|$, the hyperbolic sine function in Eq. (2.1) can be replaced by its argument to a good degree of approximation. The result is

$$J_i=\mu_iE_0\{C_i(L)-C_i(0)\exp(Z_ieE_0L/kT)\}/\{1-\exp(Z_ieE_0L/kT)\}, \quad (2.3)$$

provided that the usual identification for the zero-field mobility μ_i,

$$\mu_i=(Z_ie/kT)4a^2\nu\exp(-W/kT), \quad (2.4)$$

is made. This is the integrated form[15,20] of the ordinary linear diffusion equation[5]

$$J_i=-D_i\,dC_i/dx+\mu_iE_0C_i, \quad (2.5)$$

with the ratio μ_i/D_i given by the Einstein relation,[5]

$$\mu_i/D_i=Z_ie/kT. \quad (2.6)$$

Equation (2.3) is a valid expression for the current whenever the nonlinear effects of the electric field on the mobility current, which is fundamental to the second theory of Mott[10] and to the work of Mott and Cabrera,[11] are negligible.

Whenever E_0 approaches zero, Eq. (2.1) yields the same results as the steady-state solution of Eq. (1.1),

$$J_i=-D_i\{C_i(L)-C_i(0)\}L(t)^{-1}, \quad (2.7)$$

where D_i is given by Eqs. (2.4) and (2.6). Equation (2.7) is in fact a good approximation whenever E_0 is very much smaller in magnitude than $|kT/Z_ieL(t)|$. For example, $|kT/Z_ieL(t)|$ is approximately 10^5 V/cm for a monovalent ion diffusing in a 25-Å oxide film at 300°K.

2. Electronic Current

Figure 1, which represents the energy for electrons as envisioned by Mott[2] for the metal-oxide-oxygen system, is also applicable for the metal-oxide-metal system.[7–9] The major difference is that the Fermi level of the second metal replaces the O^- level of the adsorbed oxygen. Because of the similar energy diagrams, electron tunnel current expressions for the two phenomena can be developed in the same manner. Simmons,[7] for example, has derived an approximate but comparatively simple expression for the electron tunnel current in a nonsymmetrical metal-oxide-metal structure. It is assumed that with an externally applied electrical potential V, the barrier which the electrons must penetrate in tunneling through the oxide is trapezoidal; the WKB approximation[22] and an averaging technique are then used to compute the transmission coefficient. The

[22] E. Merzbacher, *Quantum Mechanics* (John Wiley & Sons, Inc., New York, 1961), Chap. 7.

temperature dependence[8] of the tunnel current (due to the kT spread in occupation probability about the Fermi level) is neglected in Simmons' approximate equation.

The 0°K situation for the tunnel current in a metal-oxide-metal system is especially simple since it represents a physical situation in which Fermi-Dirac statistics allow tunneling to occur only from the filled portion of the conduction band in one metal electrode into the empty portion of the conduction band in the other electrode. Immediately upon affixing the second electrode, there is tunneling in one direction until the Fermi levels are exactly equalized, and then no subsequent current unless the temperature is raised or a bias voltage applied. Whenever an external potential is applied to the device, current flows only in one direction. This 0°K situation for the metal-oxide-metal system is identical to the 0°K metal-oxide-oxygen situation: If $\chi_L > \chi_0$, there is tunneling from the filled portion of the conduction band of the metal which lies above the O^- level to the oxide-oxygen interface, energy being conserved by excitation of normal modes of the adsorbed oxygen. There is no tunneling from the portion of the conduction band lying below the O^- level. When the O^- level and metal Fermi level are exactly equalized, the current drops to zero. Before equilibrium of the electron current is reached, the effective bias voltage for the electron current is $e^{-1}(\chi_0-\chi_L)+E_0L$; this drops to zero when an electron-current equilibrium is achieved, with a contact potential (Mott potential) equal to $V_M=-E_0L=e^{-1}(\chi_0-\chi_L)$ then present across the film.

The equations of Simmons are based on the assumption that the Fermi levels in the two different metals have equalized before the external field is applied. The potential effective for producing a net tunnel current in the case presently under discussion of a nonequilibrium system and no applied potential is simply the Mott potential V_M diminished by the actual electrical potential difference across the film created by the system in the attempt to achieve equilibrium. Therefore, for our purposes, V in Eq. (13) of Ref. 7 must be replaced by $V_M+E_0L(t)$, equal to $e^{-1}(\chi_0-\chi_L)+E_0L(t)$, and the following expression is obtained for the electron tunnel current:

$$J_e=\{8\pi^2\hbar L(t)^2\}^{-1}[\{2\chi_0+eE_0L(t)\}\exp\{-2m^{1/2}\hbar^{-1}L(t)\times[2\chi_0+eE_0L(t)]^{1/2}\}-\{2\chi_L-eE_0L(t)\}\times\exp\{-2m^{1/2}\hbar^{-1}L(t)[2\chi_L-eE_0L(t)]^{1/2}\}]. \quad (2.8)$$

The condition that the net current be zero whenever $-E_0L(t)$ is equal to the Mott potential $e^{-1}(\chi_0-\chi_L)$ is satisfied; this corresponds to a current equilibrium of the electronic species. For E_0 equal to zero and for χ_L considerably larger (several tenths of an electron volt or so) than χ_0, Eq. (2.8) reduces to the simple form given by Eqs. (1.2)–(1.4). Thus Eq. (2.8) inherently contains

(a) the effect of a built-in electric field on the electron tunnel current arising from the modification of the barrier shape, and

(b) the capability of describing an electron tunnel-current equilibrium.

The situation in which χ_L is larger in magnitude than χ_0 (i.e., V_M is negative and E_0 positive) may be reversed for some metal-oxide systems. Should the O^- level actually lie above the metal Fermi level ($\chi_0>\chi_L$) for a particular case, electrons could not tunnel from metal to oxygen in zero field unless thermally activated or unless a potential large enough to lower the O^- level to the metal Fermi level was first established by ionic diffusion.

The nonzero-temperature case is more complex for both the metal-oxide-metal and the metal-oxide-oxygen situations, since tunneling in both directions occurs simultaneously. The effective flux of electrons impinging upon the barrier at the oxide-oxygen interface must then be included in the derivation for the metal-oxide-oxygen case. This is given by the product of the number of filled O^- levels n_0^- and an electronic vibration frequency ν_e, where n_0^- is related linearly to the surface-charge field E_0. The reverse tunneling during an electron current equilibrium phase can reduce the magnitude of the potential by a small amount ΔV_M which is of the order of kT/e, the temperature spread in occupation probability about the Fermi level. The exact reduction depends on ν_e and n_0^-; it therefore varies somewhat with film thickness due to the variation of E_0 with $L(t)$, since E_0 and n_0^- are related linearly. The effect on the kinetics is small, even considering that the dependence of the nonlinear ionic current on V_M given by Eq. (2.1) is exponential. The growth rate is modified by a factor of the order of

$$\exp\{-|Z_iea\Delta V_M/kTL(t)|\}\simeq\exp\{-|Z_ia/L(t)|\}.$$

For monovalent cations diffusing in a film 5 monolayers in thickness, for example, $Z_ia/L(t)=0.1$; since $\exp(0.1)\simeq 0.905$, this factor represents a decrease in the ionic current of less than 10% for this situation. Due to the fact that ΔV_M depends on $L(t)$ as well as T, the kinetics would be modified slightly from the Mott-Cabrera form. This small effect is neglected in our numerical computations for the kinetics.

Besides the addition ΔV_M to the Mott potential for the case of an electron current equilibrium, there is the usual dependence of the electron tunnel current on temperature for the nonequilibrium case. This is discussed in the literature by Stratton[8] for the metal-oxide-metal case. To first order, the ratio of the current $J(T)$ at absolute temperature T to the 0°K current $J(0)$ is given by

$$J(T)/J(0)=(\pi c_1kT)/\sin(\pi c_1kT), \quad (2.9)$$

where c_1 is a parameter determined from the potential barrier. For the square barrier illustrated in Fig. 1,

$$c_1=(2m/\chi_0)^{1/2}L(t)/\hbar=4mL(t)/L_e, \quad (2.10)$$

where L_c is given by Eq. (1.4). For the effective mass m equal to the free-electron mass m_0 and for a potential barrier height χ_0 of 1 eV, $L_c \simeq 0.98$ Å and $c_1/L(t) \simeq 0.512$ (Å-eV)$^{-1}$. A film 25 Å in thickness under these conditions would have $c_1 = 12.8$ (eV)$^{-1}$, so that $J(78°\text{K})/J(0°\text{K}) \simeq 1.01$ and $J(300°\text{K})/J(0°\text{K}) \simeq 1.20$. These ratios decrease toward unity for smaller film thicknesses, smaller effective masses, and larger barrier heights.

The ratio $J(300°\text{K})/J(78°\text{K}) \simeq 1.19$ may be contrasted with the corresponding ratio $\{\exp(-\chi_0/kT_1)/\exp(-\chi_0/kT_2)\} \simeq \exp(110)$ which would be expected for the mechanism of thermionic emission over the barrier for this example. The theoretical prediction of the relatively small temperature dependence for tunneling has been verified experimentally; for example, Hartman and Chivian[9] find only a 30 to 50% increase in current in Al-Al_2O_3-Al structures with oxides approximately 26 Å in thickness upon increasing the temperature from 78 to 300°K. This dependence of the forward tunnel current on temperature is a relatively small effect, and therefore is neglected in our numerical computations.

Another possible effect which is also neglected is a spread in energy of the O^- level, corresponding to a variation in χ_L. This would result in an effect similar to the kT spread in occupation probability about the Fermi level of the second metal electrode in a metal-oxide-metal structure. The corresponding change in potential would depend primarily on the width Γ_0 of the energy distribution, and to a lesser extent, on the nature of the distribution function and the applicable statistics for the O^- levels.

It has been presumed throughout the above discussion that there is enough adsorbed oxygen at the oxide-oxygen interface to supply a sufficient number of O^- states for establishing the Mott potential. The Mott potential corresponds to approximately 1% ionization of a monolayer of neutral oxygen atoms, so this is reasonable. The present treatment presumes that the surface density of neutral physically adsorbed oxygen is essentially continuous; otherwise, geometrical factors[2,12] due to the absence of adsorbed oxygen directly opposite a certain fraction of the metal-oxide interface would have to be introduced. However, an adsorbed monolayer is a common observation even at pressures as low as 10^{-4} Torr.

3. Coupled Equations

The assumption[15] that the steady-state currents are equal in magnitude but opposite in sign leads to the following condition:

$$q_i J_i + q_e J_e = 0. \tag{2.11}$$

This condition, termed herein the "kinetic condition," is used with the currents J_i and J_e given by Eqs. (2.1) and (2.8) to determine the surface-charge field E_0 as a function of film thickness L(t). The $E_0(L)$ thus determined is substituted into either Eq. (2.1) or (2.8) to obtain the growth rate

$$dL(t)/dt = R_c J_c \tag{2.12}$$

as a function of $L(t)$. The growth rate is then integrated to yield $L(t)$ versus t. In practice, the *rate-limiting current* should be substituted into Eq. (2.12); the nearly balanced current depends too sensitively on the exact value of the field to be used. Although this rule is mandatory when making analytical approximations, it is not critical for exact numerical evaluation if enough significant figures can be handled by the computer. In the present work, the determination of $E_0(L)$ and the integration of the growth-rate equation were performed numerically[23]; Newton's method[24] was used to solve the transcendental equation for $E_0(L)$ and standard numerical techniques were employed to perform the integration.

III. NUMERICAL RESULTS

1. Dependence on Mott Potential

Figure 2 (lower part) is a linear plot of the growth curves obtained for several values of the Mott potential. The numerical values for the parameters are listed in the figure caption and Table I. The parameters q_i and q_e were chosen to be $Z_i e$ and $-e$, respectively. As previously discussed, ΔV_M was neglected in computing these curves. For values of V_M of the order of -0.75 to -0.50 V (curves 4 and 3), as postulated in the literature,[10] the film initially grows very rapidly; this phase is followed by a more or less abrupt reduction in growth rate. As V_M decreases in magnitude (e.g., curve 2,

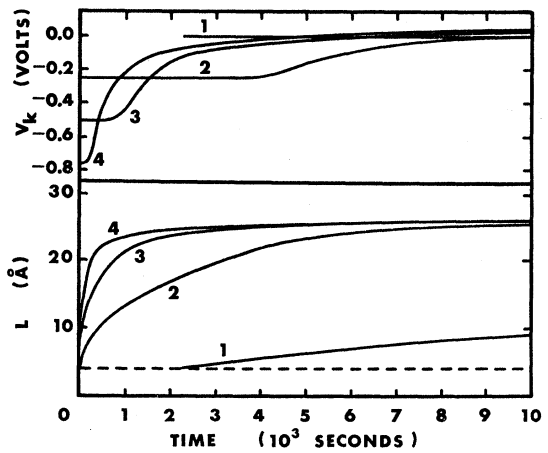

FIG. 2. Film thickness $L(t)$ and kinetic potential V_K versus time for different values of Mott potential. Curves 1–4, $V_M = 0.00$, -0.25, -0.50, and -0.75 V, respectively. Other parameters are listed in Table I.

[23] The IBM 1401-7040 computer system of Auburn University was used, with peripheral calculations performed on an IBM 1620 machine. The accuracy achieved was better than 0.1%.

[24] I. S. Sokolinkoff and R. M. Redheffer, *Mathematics of Physics and Modern Engineering* (McGraw-Hill Book Company, Inc., New York, 1953), p. 684.

TABLE I. Parameters for numerical computations.

Symbol	Definition and units	Figure 2–4	5	6	7	8
χ_0	Metal-oxide electron work function (eV)	2.00	a	2.00	a	0.64
χ_L	O^--Oxide work function (eV)	a	a	2.50	a	0.64
V_M	Mott potential $e^{-1}(\chi_0-\chi_L)$ (V)	a	−0.50	−0.50	a	0.00
T	Temperature (°K)	300	300	a	300	300
W	Thermal activation energy for ionic motion (eV)	0.65	0.65	0.65	a	a
$2a$	Ionic jump distance[b] (Å)	4.25	4.25	4.25	4.25	4.00
ν	Ionic vibration frequency (sec^{-1})	10^{12}	10^{12}	10^{12}	10^{12}	10^{12}
Z_i	Ratio of diffusing ionic defect effective charge to electronic charge magnitude e	+1	+1	+1	+1	+2
D_i	Low-field ionic diffusion coefficient $4a^2\nu\exp(-W/kT)$ (10^{-14} cm^2/sec)	2.17	2.17	a	a	a
μ_i	Low-field ionic mobility $(4a^2\nu Z_i e/kT)$ $\times\exp(-W/kT)$ (10^{-14} cm^2/V sec)	83.9	83.9	a	a	a
$C_i(0)$	Ionic defect concentration at metal-oxide interface (cm^{-3})	10^{18}	10^{18}	10^{18}	10^{18}	10^{18}
$C_i(L)$	Ionic defect concentration at oxide-oxygen interface (cm^{-3})	10^{15}	10^{15}	10^{15}	10^{15}	10^{12}
V_D	Diffusion potential $-(kT/Z_ie)\log_e\{C_i(L)/C_i(0)\}$ (V)	0.179	0.179	a	0.179	0.179
R_i	Oxide volume increase per transported ionic defect[b] (Å^3)	19.19	19.19	19.19	19.19	20.9

[a] Varied with curve in figure.
[b] The parameter R_i for Figs. 2–7 is approximately that for Cu_2O, and $2a$ is approximately the distance between Cu sites in the [100] direction in a Cu_2O lattice. This is the expected situation for diffusion in the presence of an electric field applied along the [100] direction.

$V_M=-0.25$ V), growth becomes less rapid in the early phase, which eliminates the sharp "knee" in the curve just prior to the low growth-rate phase. Note that growth under the concentration gradient alone is relatively slow (curve 1, $V_M=0$).

The corresponding electrical potential V_K across the film during growth is also shown in Fig. 2 (upper part). It is designated the kinetic potential, since it is determined at each instant by the kinetic condition of equal but opposite charge currents. Note that initially V_K has the value of the Mott potential V_M, but that it drops away as the film increases in thickness. It decreases to zero and then changes sign.

A more complete picture of the kinetics is obtained by observing the film thickness and kinetic potential versus logarithm of time in the lower part of Fig. 3 for the same growth curves. The variation of growth rate with V_M is pronounced for the early growth stages. In the later growth stages, however, it can be seen that the curves are completely independent of V_M. Although this result is at first surprising, it is readily understood by referring to the time dependence of the kinetic potential which is illustrated in the upper part of Fig. 3. It can be seen that the larger the value chosen for a negative V_M, the more quickly the potential drops toward zero, and after a relatively long time the kinetic potential is completely independent of V_M. An additional curve (dashed) is also shown in this figure to illustrate the effect of a positive Mott potential ($V_M=+0.10$ V). The computations for this curve were performed on the assumption that a diffusion potential of 0.10 V can be established by the ionic species to equilibrate the O^- level with the metal Fermi level so that tunneling can occur. This potential seriously retards ionic diffusion in the early growth stages, as evidenced by the time dependence of the dashed curve.

The behavior of the potential can be more readily understood by referring to Fig. 4. This figure is a linear plot of potential versus film thickness. Note that the

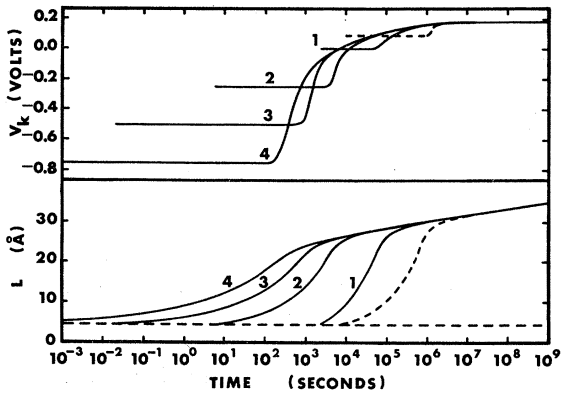

FIG. 3. Film thickness $L(t)$ and kinetic potential V_K versus logarithm of time for different values of Mott potential. Curves 1–4, $V_M=0.00$, −0.25, −0.50, and −0.75 V, respectively. Dashed curve, $V_M=+0.10$ V. Other parameters are listed in Table I.

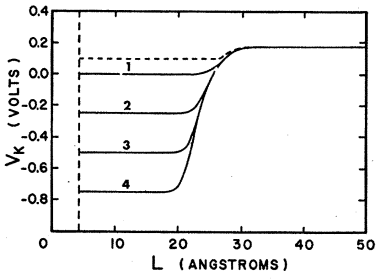

FIG. 4. Kinetic potential V_K across the film versus film thickness $L(t)$ for different values of Mott potential. Curves 1–4, $V_M=0.00$, −0.25, −0.50 and −0.75 V, respectively. Dashed curve, $V_M=+0.10$ V. Other parameters are listed in Table I.

transition away from V_M occurs at approximately 20 Å, and does not depend too markedly on the value of V_M. It is clear now that this is the thickness at which the film attenuates the electron tunnel current to such an extent that an electronic current equilibrium cannot further be maintained. The kinetic potential thus drops away from the Mott potential to values for which the ionic and electronic currents are equalized. These values, of course, vary with film thickness. Once the thickness exceeds approximately 30 Å, Fig. 4 shows that the potential is again constant, and is of the opposite sign from a negative V_M. This constant potential is the ionic diffusion potential V_D, which has a value given by $-E_{\max}{}^{(i)}L(t)$ as computed from Eq. (2.2). This region of growth corresponds to an ionic current equilibrium. The transition from electronic to ionic equilibrium is the most striking feature of the present computations.

Thus, the early stage growth is ion diffusion-current rate-limited, and the later stage growth is electronic tunnel-current rate-limited. The negative Mott potential corresponding to electronic equilibrium in the early stages aids ionic diffusion, and the diffusion potential corresponding to ionic equilibrium in the later stages aids electron tunneling. The early stage growth is faster for larger negative Mott potentials, so the critical value of approximately 20 Å for the transition is reached more quickly in time. This explains the time dependence of the potential noted in Fig. 3.

The zero-field ionic diffusion coefficient D_i and maximum ionic defect concentration $C_{\max}{}^{(i)}$ at the interfaces play important roles in the early growth stage for which Eq. (2.1) determines the rate; the time for growth to a given film thickness varies inversely with the product $D_iC_{\max}{}^{(i)}/a$, as can be deduced from Eqs. (2.1), (2.4), and (2.6). The predominant increase in rate, however, is exerted by the product $|Z_ieaV_M/kTL(t)|$, since this occurs as the argument of the hyperbolic sine function in Eq. (2.1). Temperature effects are thus especially pronounced in this phase, being exponential through D_i and $\sinh\{-Z_ieaV_M/kTL(t)\}$. Note from the argument of the hyperbolic sine function that an increase in Z_i is equivalent to a corresponding change in V_M for this early growth (pretransition) region. For example, curve 2 ($Z=1$, $V_M=-0.25$) in Fig. 2 would for $Z=2$ and $V_M=-0.25$ become almost identical to curve 3 ($Z=1$, $V_M=-0.50$). Therefore a change in Z_i results in a very large effect on the kinetics. Oxygen pressure effects will be moderate if $C_{\max}{}^{(i)}$ happens to be $C_i(L)$, and will be large if the pressure is so low that V_M cannot be sustained.

The parameters D_i, a, and V_M are entirely ineffective for the later growth stages, however, since both Eq. (2.8) for the rate-limiting electron tunnel current and Eq. (2.2) for $E_{\max}{}^{(i)}$ are independent of these parameters. The predominant rate-determining factor for the later stages of growth following the transition from electronic to ionic equilibrium is the metal-oxide electronic work function χ_0. To a lesser extent, the ionic diffusion potential $V_D=-E_{\max}{}^{(i)}L(t)$ given by Eq. (2.2) is also important in this later phase. Note from Eq. (2.2) that V_D increases linearly with temperature, inversely with Z_i, and logarithmically with the ratio of ionic defect concentrations at the interfaces. (Both $C_i(0)$ and $C_i(L)$ can vary exponentially with temperature, while only $C_i(L)$ varies significantly with oxygen pressure.) For example, consider the case in which V_D is produced by monovalent ionic defects diffusing at 300°K with boundary concentrations $C_i(0)$ and $C_i(L)$ equal to 10^{18} and 10^{15} cm^{-3}, respectively. For $\chi_0=1.00$ and $\chi_L=1.50$ eV, the electron tunnel current through 30, 35, and 40 Å films is 6.5×10^{13}, 3.8×10^{11}, and 2.1×10^{9} electrons/cm^2 sec, respectively. A factor of 2 increase in V_D results in an increase in the current (and corresponding oxide growth rate) by factors of 2.0, 4.7, and 7.0 for the 30, 35, and 40 Å films, respectively. This effect can be compared with a factor of approximately two for the corresponding increase in electron tunnel current due to the intrinsic temperature dependence arising from a spread in values of the occupation probability around the Fermi level. In general, then, the increase in rate and the temperature dependence resulting from V_D are important enough to be included in the rate constant for the later stages of growth.

2. Dependence on Metal-Oxide Work Function

The effect of varying the total barrier height χ_0, keeping V_M constant, is shown in Fig. 5. The relevant parameters are again listed in Table I. The early stage growth is unaffected by changes in χ_0, as expected because of the electron current equilibrium; however, the later-stage growth rate decreases with increasing χ_0. This reflects the fact that barrier penetration is impeded by the increased barrier height, thus yielding a lower growth rate in the electron rate-limiting stage.

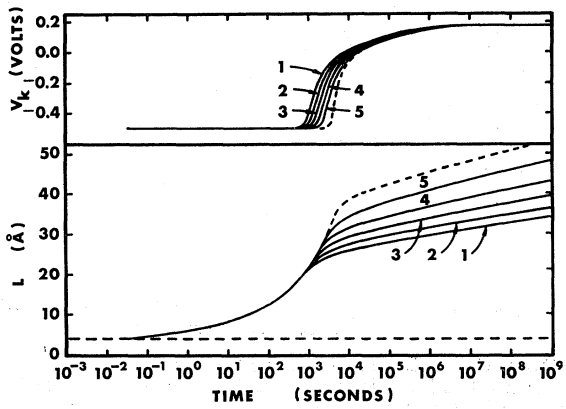

FIG. 5. Film thickness $L(t)$ and kinetic potential V_K versus logarithm of time for different values of total barrier height. Curves 1–5, $\chi_0=2.00$, 1.75, 1.50, 1.25, and 1.00 eV, respectively. Dashed curve, $\chi_0=2.00$ eV and $m/m_0=0.4$. Other parameters are listed in Table I

In curves 1–5 of Fig. 5 (as well as in the preceding figures), the electron effective mass m is considered to to be the same as the free-electron mass m_0. The dashed curve, however, is the same as curve 1 except that m is considered to be only 40% as large as m_0. Note that the greater penetrating ability of the lower mass particle yields a remarkable increase in the film thickness ($\simeq$50%) for the later stages of growth. Therefore rate can be limited by electron tunneling even for film thicknesses as large as 100 Å.

Figure 5 also shows the accompanying kinetic potential curves. Since no parameters are varied which cause a net variation in V_M and V_D, there exists little difference between the curves. The transition does occur somewhat sooner in time for the larger χ_0 curves, since the increased difficulty in achieving barrier penetration shortens the electron equilibrium phase of growth.

3. Comparison with Mott-Cabrera Theory

Figure 6 illustrates a sequence of curves which compares our coupled-current results with theoretical Mott-Cabrera curves deduced from the nonlinear ionic diffusion current of Eq. (1.5) assuming a constant V_M. The parameters for this sequence of curves are again listed in Table I. The several curves correspond to different values of the temperature, which affects the zero-field ionic diffusion coefficient and the nonlinear contributions to the current exponentially, as shown in Eqs. (1.5) and (2.1), and modifies V_D in a linear manner for fixed boundary concentrations as given in Eq. (2.2). The Mott-Cabrera type curves (primed) are characteristically[25] concave upward on the semilogarithmic plot of Fig. 6. These curves follow the coupled-current curves (unprimed) very closely during the electron tunnel-current equilibrium phase of growth. This shows that Eq. (2.1) reduces very closely to Eq. (1.5) for large

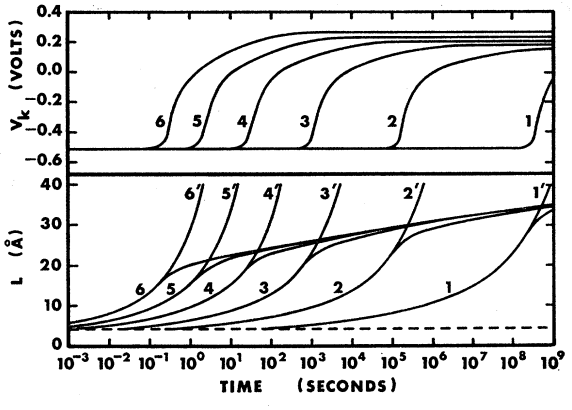

FIG. 6. Comparison of $L(t)$ versus t curves computed from nonlinear Mott-Cabrera ionic current for $V_M=-0.50$ V (primed curves) with corresponding curves for $L(t)$ and V_K deduced from coupled-currents approach (unprimed curves). Curves 1–6, T=200, 250, 300, 350, 400, and 450°K, respectively. Other parameters are listed in Table I.

[25] D. A. Vermilyea, Acta Met. 6, 166 (1958).

forward ionic currents, as expected. At the point where the kinetic potential breaks away from the constant Mott potential V_M, however, the kinetics change drastically. Because of severe attenuation of the electron tunnel current, the Mott potential can no longer be sustained. It gives way to the ionic diffusion potential, and rate is determined by electron tunneling under this potential. Instead of continuing to be concave upward, the curves become asymptotic to a straight line on the semilogarithmic plot of Fig. 6. The transition portion of the curves is convex upward. The Mott-Cabrera type curves, however, continue to rise on a logarithmic-type plot until $\sinh[-Z_i eaV_M/kTL(t)]$ can no longer be approximated by $\pm\frac{1}{2}\exp|Z_i eaV_M/kTL(t)|$, at which time they also begin to level off. This occurs at thicknesses somewhat greater than those illustrated in Fig. 6.

The difference in the results of the two approaches as illustrated in Fig. 6 has serious implications[18] regarding the magnitude of the limiting film thickness, its temperature dependence, and the sign of the electrical potential across the film when it has ceased to grow. Clearly, the limiting thicknesses following the transition are predicted to be significantly larger on the basis of the Mott-Cabrera picture than is predicted by the coupled-currents approach. In addition, the potential is generally expected to be negative (i.e., positive fields) according to the Mott-Cabrera theory, while the potential is positive following the coupled-currents transition.

The differences in time and film thickness at which the transition occurs can be seen in Fig. 6 to vary with temperature. This poses the question of whether or not the transition is expected to occur on the basis of a reasonable laboratory time scale for a given metal-oxide system. Our computations show that the time to and film thickness for the transition depend critically on the zero-field ionic mobility μ_i, and therefore on the temperature. Figure 6 illustrates that the kinetic potential decreases rapidly in magnitude once the breakaway from the Mott potential takes place, so the transition point (L_M*, t_M*) is defined for convenience (although arbitrarily) in the present work as the point at which the kinetic potential differs from V_M by 5%.

Figure 7 illustrates the dependence of the time t_M* needed to reach the transition (lower solid curves) and the transition thickness L_M* (upper solid curves) on μ_i. Note from curves 1–3 that L_M* and $\ln t_M$* decrease nearly linearly with increase in $\ln\mu_i$. The only difference between curves 1 and 2 is the electron barrier height (curve 1, $\chi_0=1.5$ eV; curve 2, $\chi_0=2.5$ eV). Note that for a given mobility the logarithm of the time to the transition is decreased only a relatively small amount by the increase in χ_0, while the transition thickness is decreased significantly. (For example, for $\mu_i=10^{-12}$ cm^2/V sec, L_M* is decreased from 23.7 to 19.0 Å by an increase in χ_0 from 1.5 to 2.5 eV). The only difference between curves 2 and 3 is the Mott potential (curve 2, $V_M=-0.5$ V; curve 3, $V_M=-1.0$ V). Note that

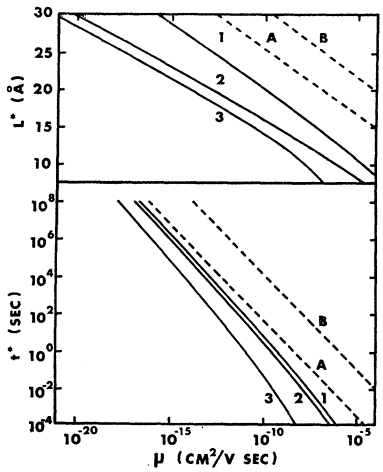

FIG. 7. Time t^* to reach transition and transition film thickness L^* as a function of zero-field ionic mobility μ_i.

Curve	χ_0(eV)	V_M(V)
1,A,B	1.5	−0.50
2	2.5	−0.50
3	2.5	−1.00

Other parameters are listed in Table I. Transition-point criteria: Curves 1–3, $V_K=0.95\ V_M$; curve A, $V_K=0$; curve B, $V_K=0.95\ V_D$.

this change exerts a small decrease in L_M^*, but a relatively larger decrease in $\ln t_M^*$. For a given mobility, then, the logarithm of the time needed to reach the transition is not too dependent on χ_0, although the transition film thickness varies somewhat with χ_0. Alternatively, the transition film thickness does not depend too critically on V_M, although the logarithm of the time to the transition does vary somewhat with V_M.

The dashed curves in Fig. 7 represent transition thicknesses and times based on different criteria for the transition point. Curve A is the same as curve 1 except that the transition point (L_0^*,t_0^*) is chosen to be the point at which V_K is zero. Similarly, curve B is the same as curve 1 except that the transition point (L_D^*,t_D^*) is chosen to be the point at which $V_K=0.95\ V_D$. Note that for a given μ_i, the increments between the transition thicknesses L_M^*, L_0^*, and L_0^*, L_D^* are approximately 5 Å. Therefore the entire transition takes place over a range of approximately 10 Å, which is a large part of the final thickness of the film. The time difference between curve 1 and curve A is a factor of 10, while there is approximately a factor of 100 separating curves A and B. Thus the entire transition covers approximately 3 orders of magnitude more time than is initially required to reach the transition.

It is perhaps helpful to delineate the range of mobility over which the transition can be expected to occur on a laboratory time scale. The area to the left of the curves in Fig. 7 is the pretransition (Mott-Cabrera) region, while the area to the right of the curves is the post-transition (coupled-currents) region. For $\mu_i>10^{-10}$ cm²/V sec in Fig. 7, t_M^* is less than 10 sec for the three curves illustrated, and L_M^* is less (generally much less) than 20 Å, while for $\mu_i<10^{-16}$ cm²/V sec, t_M^* is greater than 10^6 sec (≃12 days) and L_M^* is greater than 22.5 Å. The simple technique used to deduce the phase diagrams of Fig. 7 is described in the following section.

4. Analytical Approximations

Equation (2.12) for the growth rate can be written in the following separated form which is useful for actual evaluation of $L(t)$ versus t:

$$t=\int_0^{L(t)}\{R_cJ_c(L)\}^{-1}dL. \tag{3.1}$$

When J_c represents the nonlinear diffusion current J_i, it is generally helpful to change variables from L to L^{-1}. The early-stage $(L(t)<L_M^*)$ growth rate is given to a good degree of approximation by the nonlinear ionic current expression of Eq. (1.5), in which the concentration gradient is ignored and the potential across the film is simply V_M. Since $\{-Z_ieaV_M/kTL\}$ is of the order of unity at 300°K for $V_M=-0.5$ V across a 50 Å film with lattice parameter $2a=5$ Å and an effective ionic charge of e, it is generally a good approximation for films less than this in thickness to replace the hyperbolic sine function by one-half the corrresponding exponential function. In this limit, Rhodin[26] has pointed out that the growth-rate expression (3.1) can be integrated in terms of the tabulated exponential integral[27] $E_1(\eta)$,

$$E_1(\eta)=\int_\eta^\infty \zeta^{-1}\exp(-\zeta)d\zeta. \tag{3.2}$$

The resulting growth rate expression $L(t)$ versus t is

$$\tilde{A}t=L\exp(-\tilde{L}/L)-\tilde{L}E_1(\tilde{L}/L), \tag{3.3}$$

where

$$\tilde{A}\equiv R_in_i\nu\exp(-W/kT), \tag{3.4}$$

and

$$\tilde{L}\equiv -q_iaV_M/kT. \tag{3.5}$$

The parameter R_i is the oxide volume increase per ionic defect transported to the oxide-oxygen interface.

If a replacement of the hyperbolic sine function by the corresponding exponential function is not a good approximation in certain instances, then Eq. (1.5) can be used in Eq. (3.1) with the suggested change of variable $L(t)\rightarrow L(t)^{-1}$ to yield the following integral form of the growth equation:

$$2\tilde{A}t=\tilde{L}\int_{\tilde{L}/L}^\infty \eta^{-2}\,\mathrm{csch}\eta d\eta. \tag{3.6}$$

[26] T. N. Rhodin, Jr., J. Am. Chem. Soc. **72**, 5102 (1950).

[27] *Handbook of Mathematical Functions*, edited by M. Abramowitz and I. A. Stegun, National Bureau of Standards Applied Mathematics Series, No. 55 (U. S. Government Printing Office, Washington, D. C., 1964), p. 227.

Dignam *et al.*[28] have numerically evaluated this expression to obtain growth curves for comparison with their experimental data on oxidation of aluminum.

In the limit where $V_M=0$, the early-stage growth is parabolic:

$$L(t)\propto t^{1/2}, \tag{3.7}$$

as can be obtained by substituting Eq. (2.7) into Eq. (3.1) and performing the simple integration. This is the case, for example, in curve 1 in Figs. 2 and 3 prior to the transition. Growth is also parabolic in the limit in which nonlinear effects are negligible.[17] This can be obtained by substituting Eq. (2.3) with $E_0=-V_M/L(t)$ into Eq. (3.1) and performing the elementary integration. A similar parabolic growth law is obtained by integrating Eq. (3.1) when the hyperbolic sine function in Eq. (1.5) is replaced by its argument, as is valid in the limit of small arguments. This parabolic law was deduced by Mott and Cabrera[11]; it differs somewhat from the one obtained using Eq. (2.3) since the effect of the concentration gradient is not included. These early-stage parabolic growth laws are not generally expected to occur, since any appreciable value of V_M will introduce nonlinear effects into ionic diffusion in the very-thin-film stage. On the basis of the present model, the transition to the electron-tunneling rate-limiting phase of growth occurs before the films become thick enough for nonlinear effects to be neglected, unless the Mott potential is very small.

The transition thickness L_M^* for a given set of parameters can be ascertained from phase diagrams such as those illustrated in Fig. 7. These can be generated quite readily by substituting Eq. (2.8) for the electronic current and Eq. (2.1) for the ionic current into the kinetic condition (2.11), with $V_K=-E_0L(t)$ given by 0.95 V_M. For a given value of $L(t)$, this equation gives immediately the value of $\{\nu\exp(-W/kT)\}$ necessary to satisfy the kinetic condition, which can then be used to compute the value of μ_i from Eq. (2.4). By choosing a series of values for $L(t)$, a phase diagram for L_M^* versus μ_i such as illustrated in the upper solid curves in Fig. 7 can be plotted. The curves L_0^* versus μ_i and L_D^* versus μ_i can be deduced in a similar manner; the only difference is that the value of V_K is zero and 0.95 V_D, respectively, instead of 0.95 V_M.

The transition time t_M^* corresponding to each particular value of L_M^* can subsequently be obtained from Eq. (3.3) to a good degree of approximation, since the deviation of V_K from V_M is not important for the chosen transition-point criterion $\{V_K=0.95\ V_M\}$. Thus a phase diagram for t_M^* versus μ_i can be plotted similar to the solid curves illustrated in the lower part of Fig. 7. The curves t_0^* versus μ_i and t_D^* versus μ_i illustrated by the lower dashed curves in Fig. 7 cannot be obtained so readily; it is necessary to do an exact integration of the growth curve to the points L_0^* and L_D^*, respectively, using the coupled-currents approach presented herein.

During the later-stage growth $[L(t)>L_D^*]$ following the transition, the growth law is almost direct-logarithmic $[L(t)\propto\log t]$, as can be noted in Figs. 3, 5, and 6. This can also be ascertained analytically by substituting the constant $\{-V_D\}$ for $E_0L(t)$ in Eq. (2.8) for the rate-limiting electron tunnel current, since the forward current (i.e., the portion involving χ_0) then has the same functional dependence on $L(t)$ as the current given by Eq. (1.2), and the reverse current (i.e., the portion involving χ_L) can be ignored to a good degree of approximation. In fact, the result is identical to Eqs. (1.2)–(1.4) with the substitution of $\{2\chi_0-eV_D\}$ for $2\chi_0$. Since the major film-thickness dependence for $L(t)>L_D^*$ is given by the exponential term in Eq. (1.2) instead of the $L(t)^{-2}$ factor of Eq. (1.3), it is acceptable to approximate $L(t)^{-2}$ in Eq. (1.3) by $(L_D^*)^{-2}$ in the present case. The above approximations for J_e reduce the growth expression (3.1) to an especially simple form, which yields

$$L(t)=L_c'\ln[\exp(L_D^*/L_c')+\{A''R_e(t-t_D^*)/L_c'\}], \tag{3.8}$$

where

$$L_c'\equiv\hbar\{4m(2\chi_0-eV_D)\}^{-1/2}, \tag{3.9}$$

and

$$A''\equiv(2\chi_0-eV_D)/\{8\pi^2\hbar(L_D^*)^2\}. \tag{3.10}$$

The parameter $R_e\equiv|q_e/q_i|R_i$ is the oxide volume increase per electronic defect transported to the oxide-oxygen interface. The rate constant in the logarithmic portion of the growth curve is therefore dependent on the diffusion potential V_D, as well as the electron effective mass m and the metal-oxide work function χ_0.

5. Comparison with Published Experimental Data

The observation of initially rapid thermal oxidation followed by very slow oxidation, with effective limiting thicknesses in the range 20 to 50 Å, is very common below 30°C. This behavior has been observed even for temperatures as high as 300°C. The kinetics have been reported in some cases to be of the Mott-Cabrera (pre-transition) form,[25,26,28–31] in other cases to be of the direct-logarithmic (post-transition) form,[32–35] while in

[28] M. J. Dignam, W. R. Fawcett, and H. Böhni, J. Electrochem. Soc. **113**, 656 (1966).

[29] T. N. Rhodin, Jr., J. Am. Chem. Soc. **73**, 3143 (1951)

[30] O. Kubaschewski and B. E. Hopkins, *Oxidation of Metals and Alloys* (Butterworths Scientific Publications, Ltd., London, 1962), p. 38.

[31] M. Wym. Roberts, Trans. Faraday Soc. **57**, 99 (1961).

[32] J. Kruger and H. T. Yolken, Corrosion **20**, 29t (1964); J. Kruger (private communication).

[33] F. P. Mertens, Ph.D. dissertation, Worcester Polytechnic Institute, 1965 (unpublished). See also J. E. Boggio and R. C. Plumb, J. Chem. Phys. **44**, 1081 (1966).

[34] K. Hauffe and B. Ilschner, Z. Elektrochem. **58**, 382 (1954).

[35] W. H. Orr, Ph.D. dissertation, Cornell University, 1962 (unpublished). See also T. N. Rhodin, in *Structure and Properties of Thin Films*, edited by C. A. Neugebauer, J. D. Newkirk, and D. A. Vermilyea (John Wiley & Sons, Inc., New York, 1959), p. 87.

still others (e.g., potassium,[36] copper,[37] and sodium[38]) neither form is found to be adequate. In the case of copper, epitaxially-induced strains in the oxide have been experimentally observed[39]; these strains surely modify the growth kinetics.

Perhaps the most convincing of the data reported to be of the Mott-Cabrera form are those of Vermilyea[25] for the oxidation of polycrystalline tantalum between 150 and 300°C. Oxide film thicknesses were in the range 10 to 140 Å, and were measured with a capacitance technique. Although the scatter in the data is appreciable, the computed curves fit the data within experimental error; moreover, the temperature dependence is self-consistent with one set of values for the relevant parameters. The corresponding data taken at 50 to 100°C, however, deviate from the Mott-Cabrera form, and in fact, are better fit with a straight line on linear-thickness–versus–logarithm-of-time plots. This behavior at 50 and 100°C is not explained by the present approach, since according to Fig. 6, the transition is expected to occur sooner at higher temperatures. Also, thermionic emission may play a more important role than electron tunneling in establishing the Mott potential for the 300°C curve, since the 140-Å thickness provides a formidable barrier for tunneling even if the effective mass of the electron in the oxide is relatively low.

Rhodin[26,29] measured the kinetics of oxidation of carefully prepared monocrystals of copper at temperatures in the range 78–353°K using a vacuum microbalance. The relatively close agreement between the measured and computed curves for film thicknesses below 30 Å has on occasion been offered as evidence for the validity of the Mott-Cabrera theory. Vermilyea[25] has pointed out, however, that the data and computed curves are inconsistent with the Mott-Cabrera equation because the slope on the linear-thickness–versus–logarithm-of-time plots decreases with increasing time. The present authors have attempted to reproduce the computed linear-thickness–versus–linear-time plots in Fig. 5 of this work[26] on copper. Although the analytical expressions are correct and the values of the parameters are deduced properly from Fig. 4, the early-stage oxidation occurs much too slowly to be consistent with the short times in which the films reach a limiting thickness. In addition, the temperature dependence was not found to be self-consistent with a single set of values for the relevant parameters. It must therefore be concluded that these interesting data provide no quantitative support for the Mott-Cabrera theory. Likewise, these data do not provide quantitative support for the present coupled-currents approach because of the relatively large temperature effects observed in the later stages of growth.

Dignam *et al.*[28] found with the aid of a vacuum microbalance that the growth kinetics of amorphous oxide films 30 to 60 Å in thickness formed on polycrystalline aluminum between 450 and 500°C could be described well by the Mott-Cabrera equation. Values for the parameters were derived from a comparison between experiment and theory. Likewise, the observations of Roberts[31] using a volumetric technique for the formation of iron oxide 6 to 12 monolayers in thickness for temperatures 0 to 120°C have been interpreted as indicating the validity of some features of the Mott-Cabrera theory. The most commonly observed experimental feature which is in agreement with the Mott-Cabrera theory seems to be the linear dependence of the reciprocal of the limiting oxide-film thickness on temperature.[25,26,29,31]

The experimental data supporting the thin-film direct-logarithmic equation are in general much less subject to question than the data supporting the Mott-Cabrera equation. Kruger and Yolken[32] have measured the oxidation kinetics at 30°C on single-crystal and polycrystalline iron with an ellipsometer, and find that films 20 to 30 Å in thickness grow logarithmically over three orders of magnitude in time. Data obtained by Mertens[33] with an ellipsometer for the growth of aluminum oxide films 13 to 21 Å in thickness formed at 30°C are direct-logarithmic over four orders of magnitude in time. Hauffe and Ilschner[34] quote measurements by Scheuble for the oxidation of nickel at 200°C; growth from 10 to 18 Å is direct-logarithmic, and covers between one and two orders of magnitude in time. Orr[35] has studied the temperature dependence of the oxidation of magnesium evaporated films with the Wagener flow method. The results between −75 and 135°C indicate a later-stage growth which is direct-logarithmic, following an initial nucleation and lateral growth phase. The oxide films are of the order of 25 Å in thickness, and are insensitive to temperature and oxygen pressure, in accordance with the predictions of the present work.

Unfortunately, no experimental studies have been made which are comprehensive enough to cover both the pretransition and post-transition regions. In many cases there are factors such as low oxygen pressures[32] and nucleation phenomena[35] which limit the early-stage growth rate, thus effectively eliminating the Mott-Cabrera phase. In other cases this phase occurs so rapidly that it cannot be followed by present-day film-thickness monitoring instruments. On the other hand, the much slower growth rate in the logarithmic phase enables it to be readily observed.

Figure 8 illustrates our attempt to fit the logarithmic phase of the oxidation of iron at 30°C and 760 Torr oxygen pressure with the present coupled-currents ap-

[36] J. V. Cathcart and G. P. Smith, J. Electrochem. Soc. **107**, 141 (1960).
[37] F. W. Young, J. V. Cathcart, and A. T. Gwathmey, Acta Met. **4**, 145 (1956).
[38] J. V. Cathcart, L. L. Hall, and G. P. Smith, Acta Met. **5**, 245 (1957).
[39] B. Borie, C. J. Sparks, Jr., and J. V. Cathcart, Acta Met. **10**, 691 (1962).

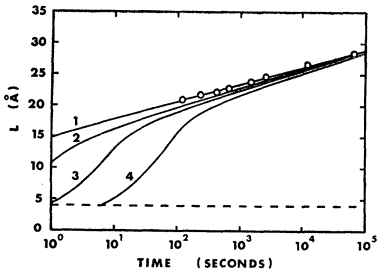

FIG. 8. Comparison of calculated oxide film thickness $L(t)$ versus logarithm of time with experimental data of Kruger and Yolken for the oxidation of iron at 300°K and 760 Torr oxygen pressure. Curves 1–4, $W=0.20$, 0.40, 0.45, and 0.50 eV, respectively. Other parameters are listed in Table I.

proach. The data are those published by Kruger and Yolken.[32] Note that curve 1 fits the data quite well. Parameters are again listed in Table I; for convenience, the values of χ_0 and V_D listed are appropriate for the situation in which $m=m_0$. In reality, the proper logarithmic slope was obtained by adjusting the quantity $(m/m_0)(2\chi_0-eV_D)$ to 1.10 eV. Smaller effective masses yield correspondingly larger values of $(2\chi_0-eV_D)$ for the given slope. The logarithmic portion of the calculated curve was matched to the experimental curve by adjusting the value for the electron flux in the metal. The theoretical value given by free-electron theory contains the pertinent factor $\{8\pi^2\hbar L(t)^2\}^{-1}$ in Eq. (2.8), which is 1.92×10^{13} (sec eV)$^{-1}$ $L(t)^{-2}$; it was necessary to reduce this factor to 3.19×10^{6} (sec eV)$^{-1}$ $L(t)^{-2}$, a reduction of approximately six orders of magnitude. The value of W chosen to compute curve 1 is 0.20 eV, and V_M is chosen to be zero for convenience. Curves 2, 3, and 4 illustrate the effect of increasing W while keeping all other parameters fixed. For these curves, $W=0.40$, 0.45, and 0.50 eV, respectively. The increase in W effectively decreases μ_i. This perturbs the slope of the logarithmic region, since for the lower zero-field mobilities the transition is extended throughout the measured range of film thicknesses. For very low mobilities, as illustrated by curve 4, there is a significant deviation of the theoretical from the experimental curve. Figure 8 therefore shows that a lower limit to the zero-field ionic mobility is provided by a comparison between theory and experiment for the case of a fixed V_M. It furthermore emphasizes the shape of the curve which is predicted for measurements taken prior to and during the transition.

IV. CONCLUSIONS

(1) Electronic tunnel-current equilibrium generally prevails in the early low-temperature growth stages for negative Mott potentials whenever $\chi_0>W$; rate is limited by an ionic diffusion current of the Mott-Cabrera form. The critical factors determining growth rate in this phase are $\sinh(Z_ieE_0a/kT)$ and $a\nu C_{\max}^{(i)}\times\exp(-W/kT)$. The increase in rate with increase of temperature is thus exponential. A smaller temperature effect in the opposite direction results from a dependence of V_M on kT due to reverse tunneling.

(2) Ionic current equilibrium prevails in the later growth stages; rate is limited by electronic tunneling under V_D, and the growth law has a nearly direct-logarithmic ($L(t)\propto\log t$) form as predicted by the first theory of Mott. The critical parameters determining growth rate in this phase are χ_0 and V_D, the quantity V_D varying with temperature and ratio of boundary concentrations as $[kT\ln\{C_i(0)/C_i(L)\}]$. An increase in V_D by a factor of two results in a severalfold increase in the rate-limiting tunnel current; this is a relatively small effect, yet it is generally larger than the intrinsic temperature dependence of the electron tunnel current.

(3) A rather sharp transition takes place between the two growth stages with increasing film thickness; this generally occurs between 20 and 30 Å depending upon the zero-field ionic mobility, and is almost independent of V_M. This transition is usually accompanied by a change in sign of the electrical potential (negative to positive) across the film.

ACKNOWLEDGMENTS

The authors wish to thank Dr. N. Cabrera for his interest in the results of this work, Dr. T. N. Rhodin for a discussion of published data for the oxidation of copper, and Dr. J. Kruger for communication prior to publication of experimental data for the thin-film oxidation of iron. The figures were carefully drawn by J. L. Johnson. We acknowledge support of this work by the Auburn University Computer Center and thank the personnel for their cooperation. The final stage of this work was supported by NASA Research Grant No. NGR-01-003-012.